On the spectral combination of satellite gravity model, terrestrial and airborne gravity data for local gravimetric geoid computation

Tao Jiang[1] and Yan Ming Wang[2]

[1]Chinese Academy of Surveying and Mapping, Beijing, China

e-mail: jiangtao@casm.ac.cn

[2]National Geodetic Survey, NOAA, Silver Spring, MD, USA

e-mail: yan.wang@noaa.gov

Abstract

One of the challenges for geoid determination is the combination of heterogeneous gravity data. Because of the distinctive spectral content of different data sets, spectral combination is a suitable candidate for its solution. The key to have a successful combination is to determine the proper spectral weights, or the error degree variances of each data set. In this paper, the error degree variances of terrestrial and airborne gravity data at low degrees are estimated by the aid of a satellite gravity model using harmonic analysis. For higher degrees, the error covariances are estimated from local gravity data first, and then used to compute the error degree variances. The white and colored noise models are also used to estimate the error degree variances of local gravity data for comparisons. Based on the error degree variances, the spectral weights of satellite gravity models, terrestrial and airborne gravity data are determined and applied for geoid computation in Texas area. The computed gravimetric geoid models are tested against an independent, highly accurate geoid profile of the Geoid Slope Validation Survey 2011 (GSVS11). The geoid computed by combining satellite gravity model GOCO03S and terrestrial (land and DTU13 altimetric) gravity data agrees with GSVS11 to ±1.1 cm in terms of standard deviation along a line of 325 km. After incorporating the airborne gravity data collected at 11 km altitude, the standard deviation is reduced to ±0.8 cm. Numerical tests demonstrate the feasibility of spectral combination in geoid computation and the contribution of airborne gravity in an area of high quality terrestrial gravity data. Using the

GSVS11 data and the spectral combination, the degree of correctness of the error spectra and the quality of satellite gravity models can also be revealed.

Key words: Airborne gravity · Error degree variance · Geoid· Satellite gravity· Spectral combination · Spectral weight · Terrestrial gravity

1 Introduction

Geoid determination using airborne gravity has been making steady progress since 1990s (Schwarz and Li 1996; Forsberg et al. 2000; Marchenko et al. 2001; Bayoud and Sideris 2003; Novák and Heck 2002; Novák et al. 2003; Olesen 2003; Hwang et al. 2007; Barzaghi et al. 2009; Hsiao and Hwang 2010; Forsberg et al 2012; Bae et al 2012; Jekeli et al. 2013; Smith et al. 2013). Hsiao and Hwang (2010) showed that the airborne gravity improves the agreement with GPS/leveling data from 9.5 to 8.7 cm in Taiwan; Bae et al. (2012) reported an improvement from 6.6 to 5.5 cm in South Korea. Forsberg et al. (2012) demonstrated a similar improvement (from 15 cm to 13 cm) in GPS/leveling comparisons in the United Arab Emirates. All computation methods used above are based on the traditional remove-restore technique with kernel truncation/modification. Smith et al. (2013) dealt with the airborne gravity data in a slightly different way. Instead of mixing the airborne data with terrestrial data in space domain using the least squares collocation, the airborne gravity data is expanded into a spherical harmonic series, then combined with the satellite gravity model GOCO02S (Goiginger et al. 2011) and EGM2008 (Pavlis et al. 2012, 2013) spectrally using empirically determined weights. This coefficient model is then used as the reference model in the traditional remove-restore fashion where the Stokes's kernel is truncated at degree and order 480.

In this paper, the spectral weights are determined from gravity data based on their distribution and spacing. The error degree variances at the lower degrees are estimated with the aid of a satellite gravity model, and at higher degrees are computed from the error covariances estimated from the local gravity data. For comparative analysis, the error degree variances of local gravity data are also estimated by using the white and colored noise models of the Royal Institute of Technology (KTH, Sjöberg 1986; Ågren 2004). The derived spectral weights are then applied to geoid computation in the southeastern Texas area. By comparing

GPS/leveling data and astrogeodetic deflections of the vertical (DoV) measured in the GSVS11 (Smith et al. 2013), the computed gravimetric geoid models are tested and evaluated.

Mathematical formulations of spectral combination are presented in section 2. Section 3 formulates the estimation of error degree variances from gravity data and the white and colored noise models. Section 4 shows the numerical results. Conclusions and discussions are given in section 5.

2 The method of spectral combination

The global gravity models (GGM) have been widely used as the reference field in the local geoid computations. The reference gravity model can be written as

$$T^{Ref}(r,\phi,\lambda)=\sum_{n=2}^{N_{Ref}}(\frac{a}{r})^{n+1}\alpha_n^{Ref}Y_n(\phi,\lambda) \tag{1}$$

where N_{Ref} is the uppermost degree of series expansion, a is the semi-major axis of the reference ellipsoid, $\alpha_n^{Ref}=(C_{nm}^{Ref}\ \ S_{nm}^{Ref})$ are the coefficient vectors, $Y_n=(\overline{R}_{nm}\ \ \overline{S}_{nm})^T$ is the transpose of the vector of normalized spherical harmonics of degree n (Heiskanen and Moritz 1967, p. 31), and r,ϕ,λ are the spherical coordinates of the computation point.

If a satellite gravity model, terrestrial and airborne gravity data are combined spectrally, the height anomaly ζ can be computed as

$$\zeta=\gamma^{-1}(T^{Coef}+\delta T^{Terr}+\delta T^{Air}) \tag{2}$$

where ζ, T^{Coef}, δT^{Terr}, δT^{Air} and γ are referred to the computation point on Earth surface, γ is the normal gravity, δT^{Terr} and δT^{Air} are the residual disturbing potential of the terrestrial and airborne gravity, respectively. They are computed by

$$\delta T^{Terr}=\iint_{\sigma}K^{Terr}(\psi)(\Delta g^{Terr}-\Delta g^{Ref})d\sigma \tag{3}$$

$$\delta T^{Air}=\iint_{\sigma}K^{Air}(\psi)(\delta g^{Air}-\delta g^{Ref})d\sigma$$

where Δg^{Terr} and δg^{Air} are the terrestrial gravity anomaly on Earth surface and the airborne gravity disturbance at flight altitude, respectively. Δg^{Ref} and δg^{Ref} are the gravity anomaly and gravity disturbance computed from an ultra-high degree GGM at Earth surface and flight altitude, respectively. The kernel functions are given by

$$K^{Terr}(\psi) = \frac{a}{4\pi} \sum_{n=2}^{N_{Terr}} \omega_n^{Terr} \left(\frac{a}{r}\right)^{n+1} \frac{2n+1}{n-1} P_n(\cos\psi) \tag{5}$$

$$K^{Air}(\psi) = \frac{a}{4\pi} \sum_{n=2}^{N_{Air}} \omega_n^{Air} \left(\frac{a}{r}\right)^{n+1} \left(\frac{a+H_{Fly}}{a}\right)^{n+2} \frac{2n+1}{n+1} P_n(\cos\psi) \tag{6}$$

where ω_n^{Terr} and ω_n^{Air} are the spectral weights for the terrestrial and airborne gravity data, respectively, H_{Fly} is the mean flight altitude. $[(a+H_{Fly})/a]^{n+2}$ is the downward continuation factor, because the airborne gravity disturbance δg^{Air} is at the flight altitude. P_n is Legendre's polynomial of degree *n*, ψ is the angular distance between computation point and current point. N_{Terr} is the maximum degree corresponding to the spatial resolution of terrestrial gravity data. N_{Air} is the maximum degree of airborne gravity contribution, which is usually smaller than N_{Terr}. Actually Eq. (5) and (6) are the degree weighted Stokes's and Hotine's kernel function.

The contribution of satellite and reference gravity model is computed by

$$\begin{aligned} T^{Coef} &= \sum_{n=2}^{N_{Sat}} \left(\frac{a}{r}\right)^{n+1} \omega_n^{Sat} \alpha_n^{Sat} Y_n \\ &+ \sum_{n=2}^{N_{Ref}} \left(\frac{a}{r}\right)^{n+1} [\omega_n^{Terr} + \omega_n^{Air}] \alpha_n^{Ref} Y_n \end{aligned} \tag{7}$$

where ω_n^{Sat} and N_{Sat} are the spectral weights and maximum degree of satellite gravity model, respectively. The last term in (7) is the contribution of the reference model, which accounts for the contribution outside the local gravity data coverage. Apparently, the reference model is used in a more complicated way than the standard remove-restore method.

The geoid model computed based on above formulas is to the spatial resolution of terrestrial gravity data. Higher spectra of the gravity field can be added by using the residual terrain model (RTM) (Forsberg 1984). Because RTM is used to add higher frequencies that exceed the maximum degree of the kernel functions (5) and (6), it can be used in a simple remove-restore fashion (e.g., Wang et al. 2012).

The geoid height can be computed from the height anomaly by

$$N = \zeta + \delta \tag{8}$$

where δ is the geoid-quasigeoid separation term (Heiskanen and Moritz, 1967, p. 326):

$$\delta \approx \frac{\Delta g_B}{\gamma} \tag{9}$$

where Δg_B is the Bouguer anomaly. Better approximation of the separation term can be found in Flury and Rummel (2009). To keep consistence with the GSVS11 geoid profile, the simple approximation Eq. (9) is used in this paper.

Neither terrestrial nor airborne gravity data are used for the determination of satellite gravity models. The errors in satellite model, terrestrial and airborne data can be assumed to be uncorrelated, thus the error degree covariances between them are zeros. Under this assumption, the spectral weights ω_n^{Sat}, ω_n^{Terr} and ω_n^{Air} can be computed by (Wenzel 1982; Sjöberg 1981)

$$\begin{aligned}
\omega_n^{Sat} &= \frac{I_n^{Sat}}{I_n^{Sat} + I_n^{Terr} + I_n^{Air}} \\
\omega_n^{Terr} &= \frac{I_n^{Terr}}{I_n^{Sat} + I_n^{Terr} + I_n^{Air}} \qquad 2 \le n \le N_{Sat} \\
\omega_n^{Air} &= \frac{I_n^{Air}}{I_n^{Sat} + I_n^{Terr} + I_n^{Air}}
\end{aligned} \tag{10}$$

$$\begin{aligned}
\omega_n^{Sat} &= 0 \\
\omega_n^{Terr} &= \frac{I_n^{Terr}}{I_n^{Terr} + I_n^{Air}} \qquad N_{Sat} + 1 \le n \le N_{Air} \\
\omega_n^{Air} &= \frac{I_n^{Air}}{I_n^{Terr} + I_n^{Air}}
\end{aligned} \tag{11}$$

$$\begin{aligned} \omega_n^{Sat} &= 0 \\ \omega_n^{Terr} &= 1 \qquad N_{Air}+1 \le n \le N_{Terr} \\ \omega_n^{Air} &= 0 \end{aligned} \tag{12}$$

where

$$I_n^{Sat} = (c_n^{Sat})^{-1},\ I_n^{Terr} = (c_n^{Terr})^{-1},\ I_n^{Air} = (c_n^{Air})^{-1} \tag{13}$$

and c_n^{Sat}, c_n^{Terr} and c_n^{Air} are the error degree variances of satellite gravity model, terrestrial and airborne gravity data, respectively. The error degree variances of satellite gravity models are usually computed from the error coefficients coming with the models. Thus only the error degree variances of terrestrial and airborne gravity data need to be estimated.

3 Error degree variance estimation

In this section, the methods of error degree variance estimation are described. Section 3.1 presents the estimation of error degree variance of terrestrial and airborne gravity data at low degrees ($n \le N_{Sat}$) with the help of satellite gravity models. Section 3.2 formulates the estimation of error degree variances at higher degrees $(n > N_{Sat})$ from gravity data directly. At the end of the section, the KTH error degree variance model is also presented (Ågren 2004, Sjöberg 1986).

3.1 Error degree variances at the low degrees

The error degree variances of terrestrial and airborne gravity at low degrees are estimated by the aid of a satellite gravity model. The observed gravity data Δg (terrestrial and airborne) and satellite gravity model Δg^{Sat} can be written as

$$\Delta g = \sum_{n=2}^{\infty} \left(\frac{a}{r}\right)^{n+2} \alpha_n^{\Delta g} Y_n = \sum_{n=2}^{\infty} \left(\frac{a}{r}\right)^{n+2} (\Delta g_n + \varepsilon_n^{\Delta g}) Y_n \tag{14}$$

$$\Delta g^{Sat} = \sum_{n=2}^{N_{Sat}} \left(\frac{a}{r}\right)^{n+2} (\Delta g_n + \varepsilon_n^{Sat}) Y_n \tag{15}$$

where Δg_n are the spherical harmonics of gravity anomaly signal, $\varepsilon_n^{\Delta g}$ and ε_n^{Sat} are the error coefficients of spherical harmonic expansion of the observed gravity anomaly and the satellite model, respectively.

The residual gravity anomaly is then

$$\begin{aligned}\Delta g^{Res} &= \Delta g - \Delta g^{Sat} \\ &= \sum_{n=2}^{N_{Sat}} (\frac{a}{r})^{n+2} (\varepsilon_n^{\Delta g} - \varepsilon_n^{Sat}) Y_n + \sum_{n=N_{Sat}+1}^{\infty} (\frac{a}{r})^{n+2} (\Delta g_n + \varepsilon_n^{\Delta g}) Y_n \end{aligned} \quad (16)$$

Up to degree N_{Sat} , the errors in the observed gravity anomaly and satellite gravity model can be considered as uncorrelated. Using the orthogonality of the surface harmonics, we obtain

$$c_n^{Res} = c_n^{\Delta g} + c_n^{Sat} \quad 2 \le n \le N_{Sat} \quad (17)$$

or

$$c_n^{\Delta g} = c_n^{Res} - c_n^{Sat} \quad 2 \le n \le N_{Sat} \quad (18)$$

where c_n^{Res} are the degree variances of the residual field computed from its spherical harmonic expansion, c_n^{Sat} are the error degree variances computed from the error coefficients of satellite gravity model.

Global harmonic analysis can only apply to global data sets (Rapp and Pavlis 1990). The terrestrial and airborne gravity data are given locally. For a global harmonic analysis, the residual gravity anomalies computed from an ultra-high degree GGM (e. g. EGM2008) and the satellite gravity model can be patched outside the local data coverage. Ellipsoidal harmonic coefficients are derived by the ellipsoidal harmonic analysis using numerical quadrature formula (Rapp and Pavlis 1990) and then transformed to spherical harmonic coefficients up to degree N_{Sat} (Jekeli 1988; Gleason 1988). The spherical harmonic coefficients are used to compute the degree variances c_n^{Res}, which are consistent with the error degree variances of satellite gravity model. For terrestrial gravity, the harmonic analysis is performed on the reference ellipsoid. The airborne gravity data are collected at the flight altitude, thus the harmonic analysis is performed on a larger ellipsoid with the major axis $a + H_{Fly}$.

3.2 Error degree variances at the medium and high degrees

The error degree variances of terrestrial and airborne gravity at higher degrees are estimated by using the method of "leave-out-one cross validation" (LOOCV). This method has been used to validate how accurately a predicative model will perform (e.g., Picard and Cook 1984; Kusche and Klees 2002). On the other hand, this method can also be used to estimate the high frequency gravity errors (e.g., Saleh et al. 2013). The procedure goes like this: excluding the point of interest, a number of nearest data points around it are used to predict the value at the point of interest. The difference between the observation and interpolated value at the point of interest is

$$\tau = \Delta g - \Delta g_{Int} \tag{19}$$

where Δg_{Int} is the interpolated gravity anomaly.

The interpolated field should be accurate at long wavelengths and canceled out in (19). Thus the discrepancy τ contains only the medium and high frequencies of errors and residual gravity signals. If we assume the high frequency errors are much larger than the residual signals at this frequency band, then the discrepancy in (19) can be considered as a good measure of medium and high frequency errors in data. This assumption was used to estimate high frequency errors in gravity data (Saleh et al. 2013), and it will be verified in the comparisons with the KTH error degree variance model in section 4.

The error covariance function can be computed by (Tscherning and Rapp 1974)

$$COV(\bar{\tau},\bar{\tau},\psi) = \frac{\sum A_i A_j \bar{\tau}_i \bar{\tau}_j}{\sum A_i A_j} \tag{20}$$

where $\bar{\tau}_i$ and $\bar{\tau}_j$ are the root mean square values of the discrepancies in each mean block whose area is A_i and A_j, respectively. The spherical distance ψ to which a special product at ψ_{ij} is determined by

$$\psi - \frac{\Delta\psi}{2} < \psi_{ij} \le \psi + \frac{\Delta\psi}{2} \tag{21}$$

where $\Delta\psi$ is the interval of spherical distance.

The error degree variances of local gravity data can be computed from the covariance function by (Heiskanen and Moritz 1967, p. 257; Wenzel 1982)

$$c_n = \frac{2n+1}{2}\beta_n^2 \int_0^\pi COV(\psi)P(\cos\psi)\sin\psi d\psi \qquad n \geq N_{Sat}+1 \tag{22}$$

where $\beta_n = 1$ for terrestrial gravity anomalies, and

$$\beta_n = (\frac{a+H_{Fly}}{a})^{n+2} \tag{23}$$

for airborne gravity disturbances at the mean flight altitude H_{Fly}.

In practice, only local data are used to compute the covariance function and the integration in Eq. (22) is truncated in an area where data are given. The truncation affects the weights at lower degree mostly. Thus the spectral weights at lower degree have to be replaced by those estimated in section 3.1.

3.3 KTH error degree variance model

Ågren (2004) used the white and colored noise models to estimate the error degree variances of local gravity data. For the white noise part, the error degree variances are given as

$$c_n^w = \frac{(2n+1)\sigma_w^2}{(N_Q+1)^2-4} \quad 2 \leq n \leq N_Q \tag{24}$$

where σ_w is the standard derivation of the white noise, N_Q is the Nyquist frequency.

For the colored noise part, the covariance function can be expressed using the reciprocal distance (Moritz 1980; Sjöberg 1986):

$$C(\psi) = \frac{\sigma_c^2}{\mu^2}[\frac{1-\mu}{1-2\mu\cos\psi+\mu^2} - (1-\mu) - (1-\mu)\mu\cos\psi]$$

where σ_c is the standard deviation of the colored noise, μ is a constant that can be computed from σ_c and the correlation length $\psi_{1/2}$ at which the covariance function has value of $C(0)/2$.

The error degree variances of colored noise are given by

$$c_n^c = \frac{\sigma_c^2}{\mu^2}(1-\mu)\mu^n \quad 0<\mu<1 \quad 2 \le n \le N_Q \tag{26}$$

The final error degree variances are then computed as

$$c_n = c_n^w + c_n^c \quad 2 \le n \le N_Q \tag{27}$$

Above formulas can be applied to airborne gravity data as well, the downward continuation needs to be considered, so the error degree variances at sea level are

$$c_n^{sea} = c_n^{Altitude}\beta_n^2 \quad 2 \le n \le N_Q \tag{28}$$

where β_n is the downward continuation factor in Eq. (23), c_n^{sea} and $c_n^{Altitude}$ are the error degree variances at sea level and flight altitude, respectively.

4 Data, computation and test

4.1 Data used and computation

For validating gravimetric geoid accuracy, the National Geodetic Survey (NGS) conducted "Geoid Slope Validation Survey of 2011" (GSVS11, Smith et al. 2013) in Texas. Along the 325 km traverse from the city of Austin to Rockport (Fig. 1), GPS derived ellipsoidal heights and spirit leveled orthometric heights were measured at 218 control marks, at 216 of the 218 stations the astrogeodetic DoVs were measured using ETH Zurich's "Digital Astronomical Deflection Measuring System" (DIADEM) (Bürki et al. 2004). The average accuracy of the differential ellipsoidal heights was 0.44 cm. The accuracy of differential orthometric heights was 1.3 cm between any pair of marks. The formal error of the surface DoVs was $0.1''$.

The gravimetric geoid is computed at a $1' \times 1'$ grid resolution over the area $27° \le \varphi \le 31°$, $261° \le \lambda \le 264°$. In order to reduce the edge effects caused by the integration of local data with a spherical cap of 2°, an enlarged data area bounded by $25° \le \varphi \le 33°$, $258.5° \le \lambda \le 266.5°$ is selected. The topography is flat in the area, and the mean and RMS value of the topographic heights are 123.9 m and 178.2 m. The mean and RMS values of the reference gravity anomalies (EGM2008) are -11.3 and 20.8 mGal, respectively. There are

29282 land gravity data and 56299 DTU13 (Andersen et al. 2013) altimetric gravity anomalies in the area. Airborne gravity was collected by GRAV-D project (Gravity for the Redefinition of the American Vertical Datum) at a mean flight altitude of 11065 m. An along track 120 second Gaussian filter had been applied to smooth out the high frequency noises in the airborne data (GRAV-D Science Team, 2012). The spatial distribution of the land, altimetric and airborne gravity data is plotted in Fig. 1. It also shows the GSVS11 survey line, the location of the city of Austin and the boundary of computation area.

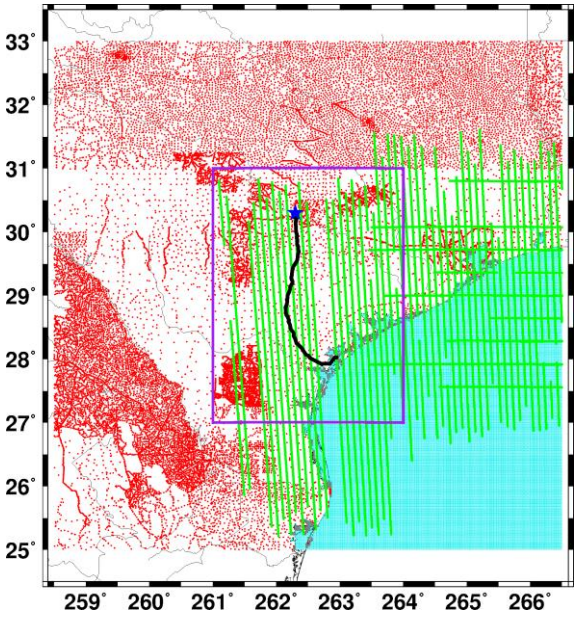

Fig. 1 Distribution of land (red), altimetric (cyan), airborne (green) gravity data, GSVS11 survey line (black), location of the city of Austin (blue star), and the boundary of computation area (purple)

Three satellite gravity models, namely GOCO03S (Mayer-Gürr et al. 2012), GO_CONS_GCF_2_DIR_R5 (DIR5) (Bruinsma et al. 2013), and GO_CONS_GCF_2_TIM_R5 (TIM5) (Brockmann et al. 2014), are used. The $3''$ Shuttle Radar Topography Mission (SRTM) elevation data (Farr et al. 2007) over the area $23° \leq \varphi \leq 35°,\ 257° \leq \lambda \leq 268°$ are used for RTM computation.

After removing EGM2008, the residual terrestrial gravity anomalies are gridded at a $1' \times 1'$ equiangular grid using program GEOGRID of the GRAVSOFT package (Tscherning et al. 1991). The residual airborne gravity disturbances with respect to EGM2008 are computed at the mean flight altitude and gridded into a $1' \times 1'$ grid. The RTM gravity effects are computed by flat-top prism integration from $3''$ detailed SRTM and $5'$ reference topography with a 100 km integration radius using program TC (Forsberg 1984). The mean and

RMS value of the RTM effects are -0.07 mGal and 4.16 mGal for terrestrial gravity anomaly, 0.73 mGal and 0.74 mGal for airborne gravity disturbance, respectively. The gridded residual terrestrial gravity anomalies and airborne gravity disturbances are inserted into Eq. (3) and (4). The radius of the spherical integration cap is empirically chosen as 2°. The maximum degree N_{Terr} in Eq. (5) is chosen as 10800 corresponding to $1'$ grid spacing of terrestrial data. The contributions of satellite gravity model and reference model are computed through Eq. (7). The RTM effects on height anomaly are restored to compensate for the removal operation. All the computations are based on the GRS80 (Geodetic Reference System 1980) ellipsoid and the tide-free system.

4.2 Combination of two data types

In this section, numerical results of the combination of two data types are presented. We start with the combination of satellite gravity models and terrestrial gravity data. This combination is the classical one for areas where airborne gravity data are not available. Then the combination of satellite models and airborne data is presented for comparison.

For estimation of the error degree variances of terrestrial gravity data below degree N_{Sat}, the residual gravity anomalies relative to satellite gravity model are averaged into $10' \times 10'$ on the GRS80 ellipsoid. Outside this area, the grids are filled with residual gravity anomalies computed from EGM2008 and satellite model. A set of spherical harmonic coefficients are computed to degree and order N_{Sat} using global harmonic analysis. The error degree variances are then computed using Eq. (18). Based on these error degree variances, the spectral weights of satellite gravity models and terrestrial gravity data below degree N_{Sat} are determined and illustrated in Fig. 3, 4, and 5.

Fig. 2 shows the error degree variances of satellite gravity models GOCO03S, DIR5 and TIM5, no error calibration applied. The error degree variances differ significantly above degree 140.

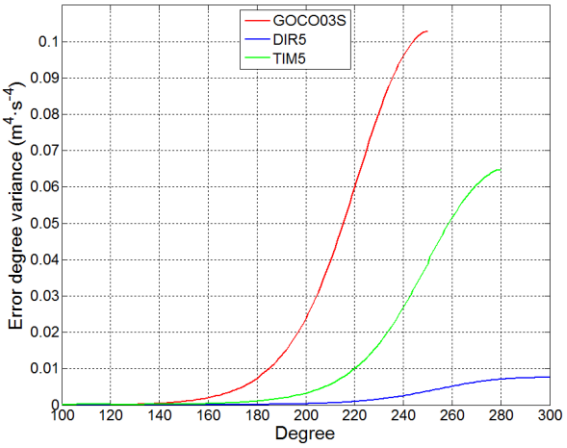

Fig. 2 Error degree variances of GOCO03S, DIR5 and TIM5

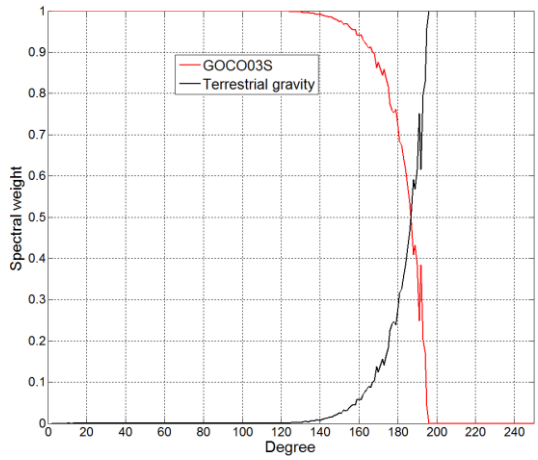

Fig. 3 Spectral weights of GOCO03S and terrestrial gravity data

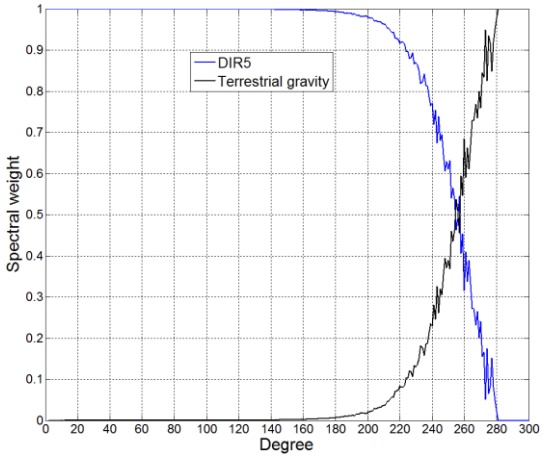

Fig. 4 Spectral weights of DIR5 and terrestrial gravity data

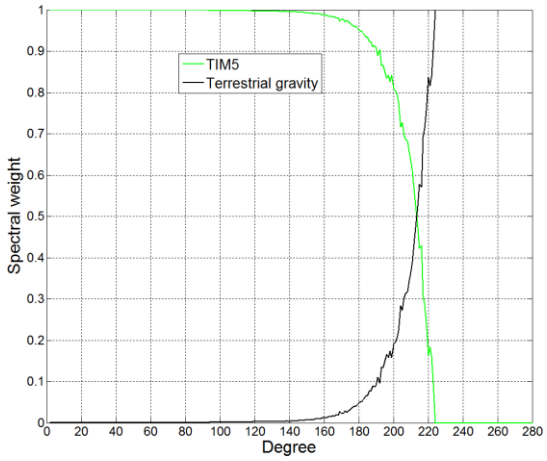

Fig. 5 Spectral weights of TIM5 and terrestrial gravity data

Once the spectral weights of satellite gravity model and terrestrial gravity data below degree N_{Sat} are determined, a gravimetric geoid can be computed by spectrally combining the two data sets without using airborne data. Note that the terms for airborne gravity in the equations of Sect. (2) and (3) should not be considered in the computation. From Fig. 3, 4 and 5, one can see that the terrestrial gravity starts contribution at degree 120, 160 and 140 for satellite gravity models GOCO03S, DIR5 and TIM5. The weights of the terrestrial data and satellite model intersect at the degree 187, 251 and 213, respectively. At these degrees, the satellite model and terrestrial gravity have equal contribution. After these degrees, the terrestrial gravity contribution increases while that of the satellite model decreases. The degrees at which the weights of each satellite model reduce to zero are 196, 281 and 224. After those degrees the terrestrial gravity takes full weight. Notice that the weights of DIR5 decrease much slower than those of GOCO03S and TIM5, yielding much more contributions from DIR5 model in the combination, this can be explained by Fig. 2 that the DIR5 modeled error degree variances are in general rather small compared with the other two satellite models.

Table 1 Statistics of the differences between gravimetric geoid models and GSVS11 GPS/leveling (unit: m)

Truncation degree	GOCO03S+Terrestrial		DIR5+Terrestrial		TIM5+Terrestrial	
N_{Sat}	Mean	Std	Mean	Std	Mean	Std
150	0.356	0.014	0.372	0.021	0.358	0.017
160	0.350	0.012	0.366	0.017	0.351	0.012
170	0.352	0.014	0.378	0.018	0.364	0.016
180	0.349	0.011	0.375	0.025	0.361	0.017
190	0.337	0.022	0.355	0.034	0.340	0.031
200	0.332	0.018	0.360	0.024	0.348	0.022

Even if the spectral weights are computed to the maximum degree of satellite models, it turns out that the truncation of satellite models at certain degree is necessary for a better geoid solution. This fact indicates: a) the potential coefficients above the truncation degree are not accurate; b) the error coefficients are not reliable at higher degrees. If they were, the truncation would be unnecessary. Table 1 lists the statistics of the differences between the computed gravimetric geoids with different truncation degree N_{Sat} and the GSVS11 GPS/leveling data. At all the truncation degrees, the GOCO03S based geoid performs better than the other two geoid models in terms of the standard deviation of differences. Although DIR5 is based on the combination of GRACE, GOCE and LAGEOS data, DIR5 performs the worst in comparison with the other two models. Notice the big differneces of the error degreee variances between the three satellite models, it suggests that the error degree variances of DIR5 model may be too optimisitc at higher degrees (Fig. 2).

The optimal truncation degree for GOCO03S is at $N_{Sat} = 180$, resulting the standard deviation of the difference of 1.1 cm with the GSVS11 data, and at $N_{Sat} = 160$ for both DIR5 and TIM5 based geoid with the standard deviation of 1.7 cm and 1.2 cm, respectively (Table 1).

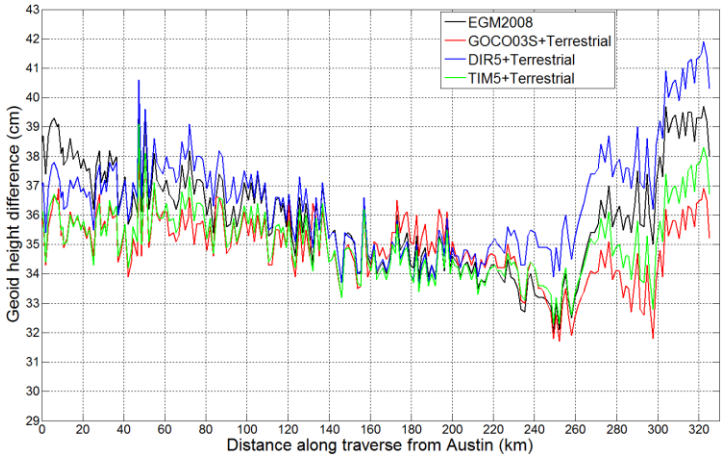

Fig. 6 Differences between terrestrial enhanced gravimetric geoids and GSVS11 GPS/leveling (unit: cm)

Fig. 6 shows the differences between the geoid models and the GSVS11 GPS/leveling data. EGM2008 geoid is also included in the comparison. The first observation from Fig. 6 is that both the EGM2008 geoid and the DIR5 based geoid have a larger slope from zero to 240 km and a large discrepancy at the end of the traverse (near shore). The GOCO03S and TIM5 based geoid models have much smaller slope and agree better with GSVS11 data near shore, indicating the

improvement in the recent satellite gravity models. The GOCO03S based geoid with $N_{Sat} = 180$ is designated 'tGeoid', where the prefix 't' indicates only use of terrestrial gravity data.

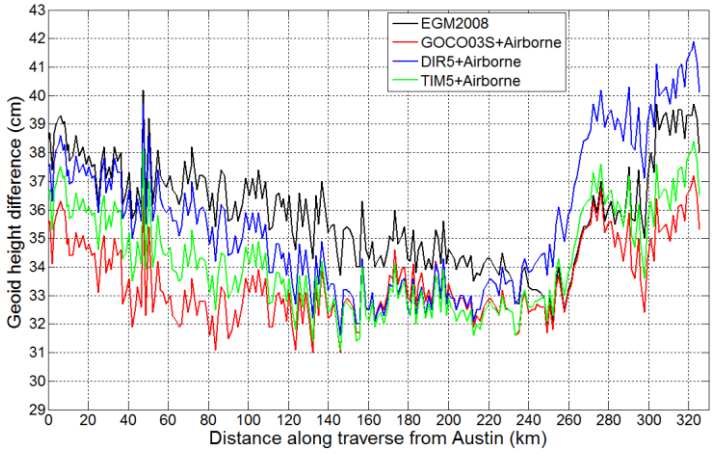

Fig. 7 Differences between airborne enhanced gravimetric geoids and GSVS11 GPS/leveling (unit: cm)

For comparison, the geoid models are also computed by combining satellite gravity model and airborne gravity data. The same procedure for spectral weighting of satellite model and terrestrial data applies to the airborne gravity data. Note that the global harmonic analysis is performed on an expanded ellipsoid with the major axis $a + H_{Fly}$ and the terms for terrestrial gravity in the equations of Sect. (2) and (3) should not be considered in the computation.

Fig. 7 plots the differences of the EGM2008 geoid and the geoid based on the combination of airborne data with each satellite model relative to the GSVS11 GPS/leveling data, respectively. The standard deviation of differences for the GOCO03S, DIR5 and TIM5 based geoid are 1.4 cm, 2.5 cm and 1.8 cm, respectively. From Fig. 6 and Fig. 7, the satellite model and terrestrial gravity combined geoid models match the GPS/leveling data much better than the geoid models derived from the combination of satellite model and airborne data. This can be attributed to the dense coverage and good quality of terrestrial data over this study area, as well as the high flight altitude of airborne data ($H_{Fly} =$ 11065 m). Therefore, the airborne data should be used as the complement rather than the substitute to the terrestrial data. Moreover, the combination results of satellite model and airborne data confirm that GOCO03S leads to the best geoid solution and DIR5 yields the worst solution among the three satellite gravity models.

One restriction of the spectral weighting at the low degrees is that a high degree GGM (e. g. EGM2008) is needed to augment the local gravity data to ensure global coverage for the estimation of global error degree variances. In the case of small local gravity data coverage, the spectral weights depend largely on the ratio of error spectra between the ultra-high degree GGM and the satellite gravity model. For the application over continental areas (e. g. the North American continent), however, the error spectra of the local gravity data are expected to be more decisive to the derived spectral weights.

4.3 Combination of satellite, terrestrial and airborne gravity

4.3.1 Spectral weight determination

Spectral weights for satellite, terrestrial and airborne gravity up to degree N_{Sat} are determined in section 4.2. The weights above N_{Sat} are determined using the LOOCV method. Program GEOGRID is employed for interpolation (Tscherning et al. 1991). The interpolation parameters NQMAX and IPWR, the number of nearest data points in each quadrant and the power of inverse distance for weighting, are determined experimentally according to the average spacing and the spatial distribution of the data set. In the study area, the average spacing between scattered land gravity points is about 7 km. The DTU13 altimetic gravity anomalies are in $1' \times 1'$ grids, about 2 km spacing. The GRAV-D airborne gravity data are given in about 140 m along track with track spacing of 10 km. The airborne data are resampled every 3 km, reducing total data points to 7934. Taking into account data spacing and distribution, the following GEOGRID interpolation parameters are chosen: NQMAX=10 & IPWR=2 for land gravity, NQMAX=40 & IPWR=1 for altimetric gravity, and NQMAX=20/30/40/50 & IPWR=1 for airborne gravity. The statistics of high frequncy errors in land, altimetric and airborne gravity data for different interpolation paramters are summarized in Table 2.

The discrepancies of terrestrial and airborne gravity data are computed at $5' \times 5'$ equiangular grids. The grids are used to compute the error covariance functions which are then used to estimate the error degree variances. The variance and correlation length of the error covariance functions of terrestrial data are 2.62 mGal^2 and 2.1°, and those of airborne data with $\text{NQMAX\_Air} = 30$ are 2.21

mGal^2 and 5°, respectively. Four sets of spectral weights for GOCO03S, terrestrial and airborne gravity data are derived. The spectral weights are plotted in Fig. 8 on the left side. For comparison, the spectral weights determined based on the KTH error degree variance model are illustrated in Fig. 8 on the right side. The parameters used for KTH model are listed in Table 3.

Table 2 Statistics of the high frequency errors in gravity data (unit: mGal)

Data type	NQMAX	IPWR	Max	Mean	RMS
Land	10	2	10.968	1.251	1.895
Altimetry	40	1	10.735	1.307	1.724
Airborne	20	1	9.350	1.010	1.410
	30	1	11.248	1.230	1.705
	40	1	12.788	1.433	1.973
	50	1	14.128	1.624	2.228

Table 3 Parameters for KTH error degree variance model

Parameter	Terrestrial	Airborne			
$\psi_{1/2}$ (°)	0.5	0.5	0.5	0.5	0.5
σ_0^w (mGal)	1	1	1	1	1
σ_0^c (mGal)	3	1.5	2.0	2.5	3.0

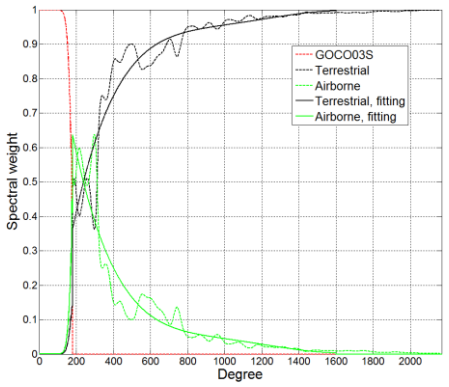

NQMAX_Air = 20

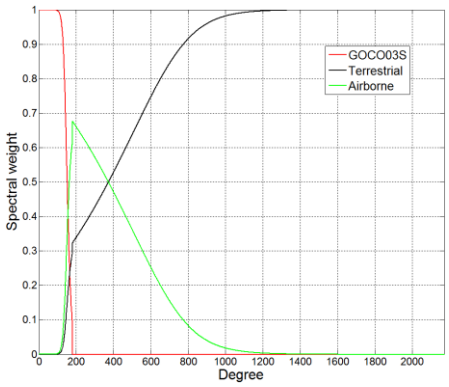

$\sigma_0^{c,Air}$=1.5

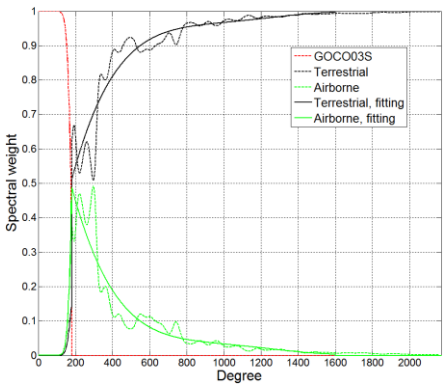

NQMAX_Air = 30

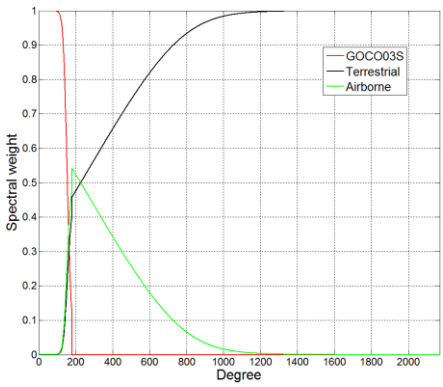

$\sigma_0^{c,Air}$= 2.0

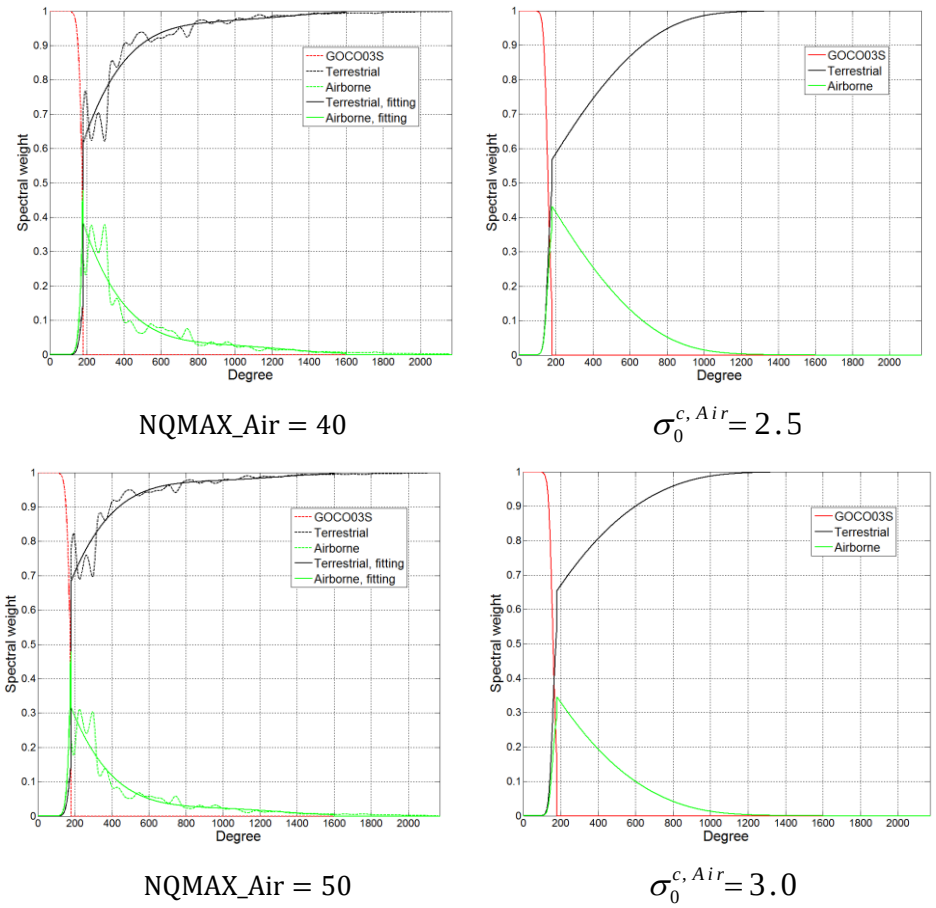

Fig. 8 Spectral weights of GOCO03S, terrestrial and airborne gravity data (left: from data; right: from KTH model)

Oscillations in the weights of terrestrial (black dash line) and airborne (green dash line) gravity are the feature of gravity data. In spite of the oscillations, the broad shape and trend are clear, the weights of airborne gravity fast decrease to the level below 0.1 due to the attenuation effect of flight altitude. To remove the local oscillations, a 5^{th} order polynomial fitting to the spectral weights above degree 180 is performed and used in later geoid computations.

The spectral weights determined from KTH error degree variance model have the same shape and similar magnitude as those derived from the local data. The good agreement shows that the KTH error degree variance model could be realistic if proper parameters are chosen. On the other hand, the good agreement verifies also that high frequency errors estimated by using LOOCV method should be representative.

The KTH error degree variance model needs a priori standard error σ_0^w and σ_0^c of each data set which are selected quite subjectively, if there is no independent data available. For the spectral weights determined from data, the

error degree variances are estimated from the data set itself and the parameters NQMAX and IPWR can be determined based on the average spacing and spatial distribution of each data set.

The spectral weights determine the contribution of each data set spectrally. Take the spectral weights with $\mathrm{NQMAX\_Air} = 30$ for example, the weights of airborne gravity (green solid line) smoothly decrease from 0.49 at degree 181 to zero after degree 1600, and those of terrestrial gravity (black solid line) increase from 0.51 to 1 symmetrically. Thus the maximum degree N_{Air} in Eq. (6) for airborne gravity should be 1600, yielding full weighted terrestrial gravity contribution above degree 1600. Another observation from Fig. 8 (left) is that most contributions from the airborne gravity are at the medium wavelengths between degree 160 and 550 approximately, while terrestrial gravity covers the medium and short wavelengths of gravity field.

4.3.2 Downward continuation stabilization

The downward continuation of airborne gravity data is an unstable process. The Tikhonov regularization (Tikhonov 1963) is often used. In this study, the regularization is not needed and the stabilization of the process is naturally done by using the spectral weights.

Fig. 9 shows the original and spectrally weighted Hotine's kernel functions (maximum degree 1600) by spherical distance at sea level. It shows that the weighted kernel gradually converges to zero, while the original kernel swings largely around zero. This downward continuation effect can also be demonstrated more effectively if the Hotine's kernel functions at $\psi = 1°$ are plotted as a function of expansion degree (Fig. 10).

Fig. 10 illustrates the unstable nature of the downward continuation, especially at high degrees. Without the spectral weights, the Hotine's kernel function fluctuates, and the magnitude of swinging increases exponentially with higher degrees – the reason for divergence of the downward continuation. After applying the spectral weights, the Hotine's kernel function goes to zero gradually at high degrees. Notice that the spectral weights are determined from gravity data and the downward continuation is optimally stabilized. This method has advantages over other methods, such as the Tikhonov regularization in which the

stabilization parameters are chosen empirically and the choices sometimes are quite artificial and time consuming (Wang et al. 2007).

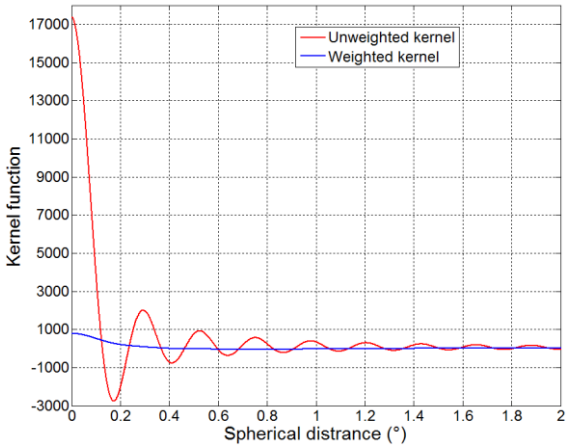

Fig. 9 Hotine's kernel functions by spherical distance with $N_{Air} = 1600$

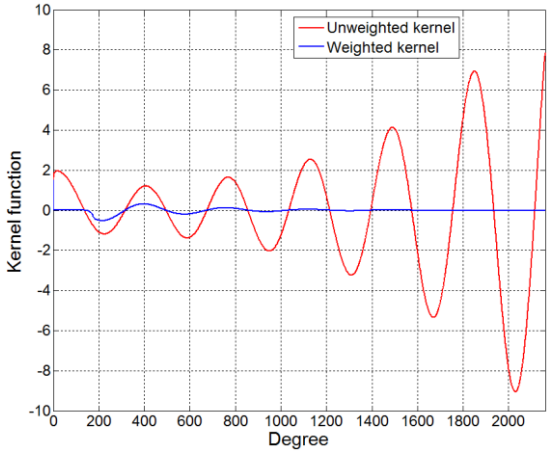

Fig. 10 Hotine's kernel functions by expansion degree at $\psi = 1°$

4.3.3 Geoid model validation

Applying the spectral weights derived above (Fig. 8), eight gravimetric geoid models are computed. Table 4 presents the statistics of the differences between the geoid models and the GSVS11 GPS/leveling derived geoid heights. The parameters NQMAX_Air and $\sigma_0^{c,Air}$ are given in the first and fourth column. It can be seen that the data driven and KTH spectral weighting yield nearly identical geoid solutions in terms of the standard deviations, though there are 5~7 mm biases between the geoid models computed based on the two spectral weighting method. For each parameter, the agreement between the geoid model and GPS/leveling data is better 1 cm. The numerical results confirm the validity and stability of the data driven and the KTH spectral weighting method for geoid computation.

Table 4 Statistics of the differences between gravimetric geoids and GSVS11 GPS/leveling (unit: m)

NQMAX_Air	Mean	Std	$\sigma_0^{c,Air}$ (mGal)	Mean	Std
20	0.343	0.009	1.5	0.348	0.010
30	0.344	0.008	2.0	0.350	0.009
40	0.344	0.009	2.5	0.351	0.009
50	0.346	0.010	3.0	0.352	0.010

The gravimetric geoid models with NQMAX_Air=30 and $\sigma_0^{c,Air} = 2.0$ are designated 'aGeoid' and 'aGeoid-KTH', respectively. The prefix 'a' stands for geoid models combined with airborne and terrestrial data. Fig. 11 plots the geoid height differences between the aGeoid and the tGeoid. The minimum and maximum of the differences are -3.3 cm and 4.6 cm, which reflect the improvement brought by airborne gravity over this area. According to Fig. 8 (left, NQMAX_Air = 30), the contributions of airborne data concentrate at the spectral bands between degree 160 and 550. Moreover, the addition of airborne gravity also results in changes of the spectral weights of satellite gravity model between degree 120 and 180 (Fig 3 vs. Fig 8), hence long wavelength features can be observed in the discrepancies.

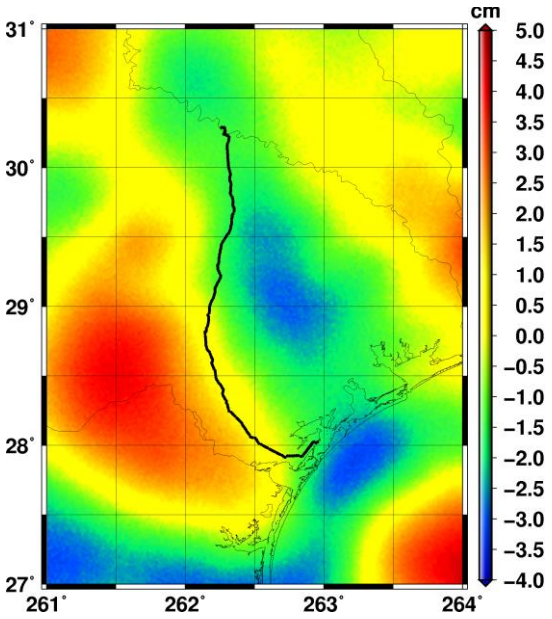

Fig. 11 Geoid height differences between the aGeoid and the tGeoid (Min = -3.3, Max = 4.6, Mean = 0.1, Std = 1.7, unit: cm)

Fig. 12 plots the differences of EGM2008 geoid, xUSGG2011, tGeoid, aGeoid and aGeoid-KTH with respect to the GSVS11 GPS/leveling derived geoid heights. Table 5 summarizes the statistics of these differences. The xUSGG2011 is a gravimetric geoid computed by Smith et al. (2013) based on remove-compute-restore method and Stokes's kernel modification. A GGM derived by empirically blending GOCO02S (Goiginger et al. 2011), EGM2008 and GRAV-D airborne

gravity data in Texas was employed as its reference model. After the incorporation of airborne gravity data, the standard deviation of the differences for the aGeoid decreases to 0.8 cm, which is slightly better than xUSGG2011 (std = 0.9 cm) and the aGeoid-KTH (Std = 0.9 cm). From Fig. 12, one can see that the deviations in the curve of tGeoid disappear in that of aGeoid, especially over the coastal area (after 280 km), indicating the improvement of accuracy due to the inclusion of airborne gravity data. The differences for the aGeoid are quite random and close to a constant value relative to the GPS/leveling derived geoid heights, while the curves of the xUSGG2011 and aGeoid-KTH exhibit gentle downward slopes which indicate small systematic errors. Notice the bias around 0.35 m between all the gravimetric geoid models and the GPS leveling derived geoid heights, this is because of the different W_0 values adopted by the gravimetric geoid model and the North America Vertical Datum 1988.

Table 5 Statistics of the differences between gravimetric geoids and GSVS11 GPS/leveling (unit: m)

Model	Min	Max	Mean	Std
EGM2008	0.319	0.401	0.360	0.018
xUSGG2011	0.320	0.393	0.355	0.009
tGeoid	0.317	0.385	0.349	0.011
aGeoid	0.313	0.373	0.344	0.008
aGeoid-KTH	0.314	0.384	0.350	0.009

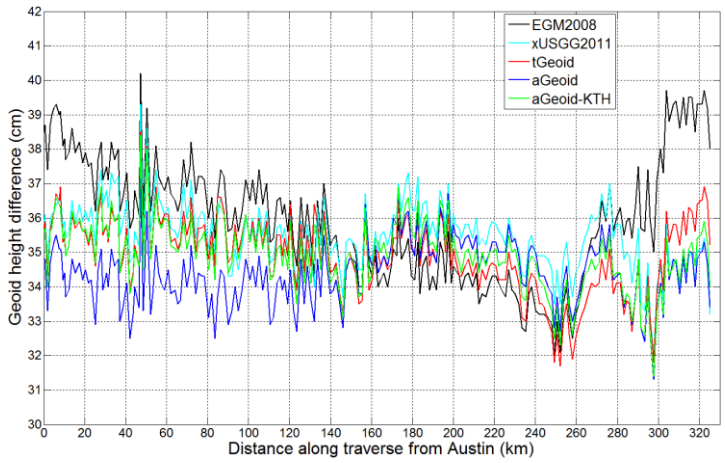

Fig. 12 Differences between gravimetric geoids and GPS/leveling along GSVS11 survey line (cm)

The DoVs derived from the five geoid models are also compared with the GSVS11 DoV measurements. The north-south and west-east components of DoVs on the geoid are computed by cubic spline from the geoid models. To facilitate the comparisons, the 216 surface DoVs measured by the DIADEM are reduced to the geoid by applying the correction corresponding to topographic height anomaly-to-geoid correction. Table 6 presents the statistics of the differences in DoVs on the

geoid between these geoid models and GSVS11 measurements. The standard deviations of the discrepancies between the modeled DoVs and measured DoVs range from 0.19″ to 0.22″for the north-south components and from 0.19″ to 0.23″ for the west-east components. What we can observe from Table 6 is that the addition of airborne data only slightly improves the match between modeled DoVs and measured DoVs.

Table 6 Statistics of the differences in DoVs on the geoid between gravimetric geoids and GSVS11 measurements (unit: arcsec)

Model	North-South (ξ)				West-East (η)			
	Min	Max	Mean	Std	Min	Max	Mean	Std
EGM2008	-0.66	0.46	-0.08	0.22	-0.52	0.54	-0.05	0.23
xUSGG2011	-0.60	0.48	-0.07	0.20	-0.57	0.57	0.03	0.19
tGeoid	-0.66	0.55	-0.06	0.20	-0.52	0.75	0.06	0.23
aGeoid	-0.64	0.49	-0.06	0.19	-0.55	0.62	0.06	0.21
aGeoid-KTH	-0.52	0.69	-0.05	0.20	-0.60	0.70	0.08	0.22

5 Conclusions and discussions

The spectral combination for geoid computation is tested in southwest Texas area. The spectral weights of terrestrial and airborne gravity data are determined from the gravity data directly. As a comparison, the KTH error degree variance model is also used to determine the spectral weights. Numerical results show not only the spectral weights, but also the geoid models computed from both methods are very close, even if the weights are determined in quite different ways. The good agreement between the spectral weights determined from gravity data and KTH error degree variance model implies that both methods capture the same error characteristics in different data sets, and the high frequency error estimated from data using LOOCV method should be realistic.

The spectral weights from data are determined based on the average spacing and distribution of each data set. The spectral weight determination by the KTH error degree variance model requires a priori information of the errors in gravity data, which is assigned empirically – sometimes can be quite subjective if there is no independent data set available.

Using the derived spectral weights, the gravimetric geoid by combining GOCO03S, terrestrial (land and altimetric) gravity agrees with GSVS11 GPS/leveling data in ±1.1 cm in terms of standard deviation. The addition of GRAV-D airborne gravity data collected at 11 km altitude improves the agreement to ±0.8 cm over the 325 km traverse. The slight improvement over

xUSGG2011 (±0.9 cm) may be attributed to the better satellite gravity model (GOCO03S vs. GOCO02S) and improved spectral weighting scheme. The closeness of the results demonstrate the fact that whether the combination of different data sets is done using spherical harmonic series (xUSGG2011) or by local Stokes's/Hotine's surface integration in this paper, the results agree in mm level.

A big advantage of spectral combination is the downward continuation stabilization of airborne gravity data. Since the spectral weight of airborne gravity quickly reduces to zero with increasing degree, it suppresses the high frequencies of airborne data and guarantees a stable geoid solution. The spectral combination method can also reveal the degree of correctness of the satellite gravity model and its error coefficient estimation. This method, combined with an independent high accuracy data set, such as GSVS11, can be useful for validating satellite gravity models and calibrating their error coefficients.

This study was performed in a flat area with high quality terrestrial gravity data. For areas with rough topography and large variation of gravity field, such as in the Rocky Mountains, this approach will be tested when high quality independent data sets become available.

Acknowledgments Tao Jiang is funded by the China Scholarship Council and the National Natural Science Foundation of China (No. 41204008). NGS also provided partially support for this study. The authors thank Mr. Jarir Saleh for his constructive suggestions and discussions. Drs. Jonas Ågren, Jianliang Huang, Simon Holmes and Xiaopeng Li are greatly appreciated for their constructive comments and discussions.

References

Ågren J (2004) Regional geoid determination methods for the era of satellite gravimetry. PhD dissertation, Royal Institute of Technology

Andersen O, Knudsen P, Kenyon S, Factor J, Holmes SA (2013) The DTU13 Global marine gravity field – first evaluation. Ocean Surface Topography Science Team Meeting, Boulder, Colorado

Bae TS, Lee J, Kwon JH, Hong CK (2012). Update of the precision geoid determination in Korea. Geophysical Prospecting 60 (3): 555-571

Barzaghi R, Borghi A, Keller K, Forsberg R, Giori I, Loretti I, Olesen AV, Stenseng L (2009). Airborne gravity tests in the Italian area to improve the geoid model of Italy. Geophysical Prospecting 57 (4): 625-632

Bayoud FA, and Sideris MG (2003). Two different methodologies for geoid determination from surface and airborne gravity data. Geophys J Int 155: 914-922

Brockmann JM, Zehentner N, Höck E, Pail R, Loth I, Mayer-Gürr T and Schuh W (2014). EGM_TIM_RL05: An independent geoid with centimeter accuracy purely based on the GOCE mission. Geophysical Research Letters, 41 (22): 8089-8099

Bruinsma SL, Förste C, Abrikosov O, Marty JC, Rio MH, Mulet S and Bonvalot S (2013). The new ESA satellite-only gravity field model via the direct approach. Geophysical Research Letters, 40 (14): 3607-3612

Bürki B, Müller A, Kahle H-G (2004) DIADEM: the new digital astronomical deflection measuring system for high-precision measurements of deflections of the vertical at ETH Zurich. IAG GGSM2004 Meeting in Porto, Portugal

Farr TG, Rosen P, Caro E, Crippen R, Duren R, Hensley S, Kobrick M, Paller M, Rodriguez E, Roth L, Seal D, Shaffer S, Shimada J, Umland J, Werner M, Oskin M, Burbank D, Alsdorf D (2007) The shuttle radar topography mission. Rev Geophys 45(2)

Flury J, Rummel R (2009) On the geoid-quasigeoid separation inmountain areas. J Geod 83: 829-847

Forsberg R (1984) A study of terrain reductions, density anomalies and geophysical inversion methods in gravity field modelling. Reports of the Department of Geodetic Science and Surveying, #355. The Ohio State University, Columbus, Ohio

Forsberg R, Olesen A, Bastos L, Gidskehaug A, Meyer U, Timmen L (2000). Airborne geoid determination, Earth Planets Space 52: 863-866

Forsberg R, Sahrum S, Alshamsi A and Din AHM (2012) Coastal geoid improvement using airborne gravimetric data in the United Arab Emirates. International Journal of Physical Sciences, 7(45): 6012-6023

Gleason DM (1988) Comparing ellipsoidal corrections to the transformation Between the geopotential's spherical and ellipsoidal spectrums. Manuscript Geodaetica 13: 114-129

Goiginger H, Rieser D, Mayer-Guerr T, Pail R, Schuh W.-D, Jäggi A, Maier A (2011) The combined satellite-only global gravity field model GOCO02S. European Geosciences Union General Assembly 2011, Wien

GRAV-D Science Team (2012) “Gravity for the Redefinition of the American Vertical Datum (GRAV-D) Project, Airborne Gravity Data; Block CS03”. Available 10/5/2014. Online at: http://www.ngs.noaa.gov/GRAV-D/data_products.shtml

Heiskanen WA and Moritz H (1967) Physical geodesy. Freeman, San Francisco

Hsiao YS, Hwang C (2010). Topography-Assisted downward Continuation of Airborne Gravity: An Application for Geoid Determination in Taiwan. Terr Atmos Ocean Sci 21 (4): 1-11

Hwang C, Hsiao YS, Shih HC, Yang M, Chen KH, Forsberg R, Olesen AV (2007) Geodetic and geophysical results from a Taiwan airborne gravity survey: data reduction and accuracy assessment. J Geophys Res - Solid Earth 112, B04407. doi: 10.1029/2005JB004220

Jekeli C (1988) The exact transformation between ellipsoidal and spherical harmonic expansions. Manuscripta Geodaetica 13(2): 106-113

Jekeli C, Yang HJ, Kwon JH (2013) Geoid Determination in South Korea from a Combination of Terrestrial and Airborne Gravity Anomaly Data. Journal of the Korean Society of Surveying, Geodesy, Photogrammetry and Cartography 31 (6-2): 567-576

Kusche J, Klees R (2002). Regularization of gravity field estimation from satellite gravity gradients. J Geod 76: 359-368

Marchenko AN, Barthelmes F, Meyer U, Schwintzer P (2001): Regional Geoid Determination: an application to airborne gravity data in the Skagerrak. Scientific Technical Report STR. Potsdam : Deutsches GeoForschungsZentrum GFZ, 48 S. p.

Mayer-Gürr T et al. (2012) The new combined satellite only model GOCO03s. Presentation at GGHS 2012, Venice, 2012

Moritz H (1980) Advanced physical geodesy. Herbert Wichmann Verlag, Karlsruhe

Novák P, Heck B (2002) Downward continuation and geoid determination based on band-limited airborne gravity data. J Geod 76: 269-278

Novák P, Kern M, Schwarz KP, Sideris MG, Heck B, Ferguson S, Hammada Y, Wei M (2003). On geoid determination from airborne gravity. J Geod 76: 510-522

Olesen AV (2003). Improved airborne scalar vector gravimetry regional gravity field mapping and geoid determination. Technical report, National Survey and Cadastre (KMS), Copenhagen, Denmark

Pavlis NK, Holmes SA, Kenyon S, and Factor JK (2012) The development and evaluation of the Earth Gravitational Model 2008 (EGM2008). J Geophys Res 117: B04406

Pavlis NK, Holmes SA, Kenyon SC, and Factor JK (2013) Correction to "The Development and Evaluation of the Earth Gravitational Model 2008 (EGM2008)". J Geophys Res 118 (5): Page 2633

Picard RR and Cook RD (1984) Cross-Validation of Regression Models, Journal of the American Statistical Association 79 (387): 575-583

Rapp RH and Pavlis NK (1990) The development and analysis of geopotential coefficient models to spherical harmonic degree 360. J Geophys Res 95(B13): 21885-21911

Saleh J, Li XP, Wang YM, Roman DR, Smith DA (2013) Error analysis of the NGS' surface gravity database. J Geod 87: 203-221

Schwarz KP, Li Y (1996). What can airborne gravimetry contribute to geoid determination? J. Geophys. Res. 101(B8):17 873-17 881

Sjöberg LE (1981) Least-squares combination of satellite and terrestrial data in physical geodesy. Ann Geophys, 37: 25-30

Sjöberg, LE (1986) Comparison of Some Methods of Modifying Stokes' formula. Boll Geod Sci Affini 45(3): 229-248

Smith DA , Holmes SA, Li XP, Guillaume S, Wang YM, Bürki B, Roman DR, Damiani TM (2013) Confirming regional 1 cm differential geoid accuracy from airborne gravimetry: the Geoid Slope Validation Survey of 2011. J Geod 87: 885-907

Tikhonov AN (1963) Regularization of incorrectly posed problems. Sov Math Dokl 4: 1035–1038

Tscherning CC, Rapp R (1974) Closed covariance expressions for gravity anomalies, geoid undulations, and deflections of the vertical implied by anomaly degree variance models. Reports of the Department of Geodetic Science and Surveying, #208. The Ohio State University, Columbus, Ohio

Tscherning CC, Knudsen P, Forsberg R (1991) Description of the GRAVSOFT package. Technical Report, Geophysical Institute, University of Copenhagen

Wang YM, Roman DR and Saleh J (2007) Analytical Downward and Upward Continuation Based on the Method of Domain Decomposition and Local Functions, VI Hotine-Marussi Symposium on Theoretical and Computational Geodesy, Volume 132 of the series International Association of Geodesy Symposia, edited by Peiliang Xu, Jingnan Liu, Athanasios Dermanis, pp 356-360.

Wang YM, Saleh, J, Roman DR (2012) The US Gravimetric Geoid of 2009 (USGG2009): model development and evaluation. J Geod 86: 165-180

Wenzel HG (1982) Geoid computation by least-squares spectral combination using intergral kernels. In: Proceedings of the General IAG Meeting, Tokyo, pp 438-453